Titile: Early-Stage Identification and Pathological Development of Alzheimer's Disease Using Multimodal MRI

Short title: Machine learning study of Alzheimer's Disease

Abstract:

Alzheimer's disease (AD), one of the most common progressive and irreversible neurodegenerative diseases, is estimated to affect tens of millions of people worldwide. Currently, there is still no cure for AD patients. Therefore, the study of the pathological mechanism of AD and early-stage diagnosis is essential and important. Subjective cognitive decline (SCD), as the first at-risk stage of AD occurring prior to amnestic mild cognitive impairment (aMCI), is of great research value and has gained our interest. By using diffusion tensor imaging and resting-state functional connectivity magnetic resonance imaging as powerful tools, many studies have shown the structural and functional network impairment in SCD patients. Despite all of this, the developmental mechanism from SCD, the preclinical stage of AD, to AD is still not clear. To investigate the entire pathological development of AD pathology efficiently, we proposed a machine learning classification method based on a multimodal support vector machine (SVM) to investigate the structural and functional connectivity patterns of the three stages of AD (SCD, aMCI, and AD). In addition to this, we tried to identify a potential biomarker of SCD patients that could aid in early-stage diagnosis of AD. We employed multiple binary classification experiments to distinguish three groups of patients from healthy controls. A k-fold cross-validation method was applied to estimate the generalization performance of the classification algorithm. Our experiments achieved an accuracy of 98.58% in the AD group, 97.76% in the aMCI group and 80.24% in the SCD group. Moreover, we counted the most discriminating brain regions in our experiments, which were mainly located in the default mode network (DMN) and subcortical structures (SCS). The hippocampus, the precuneus and the medial prefrontal cortex (mPFC), which exhibited high discriminative power in the classification, are typical DMN regions. The putamen and the thalamus are also discriminating brain regions and are typical of SCS as well, thereby indicating the importance of these two kinds of regions. Notably, with the development of AD pathology, SCS regions have become increasingly more important, and structural connectivity has shown more discriminative power than functional connectivity, which showed more discriminative power in the SCD group. The current study may shed new light on the pathological mechanism of AD and suggests that whole-brain structural and functional connectivity may provide potential effective biomarkers for the early-stage diagnosis of AD.

Keywords:

Alzheimer's disease, Multimodal MRI, Subjective cognitive decline, Diffusion tensor imaging, Resting-state fMRI.

Abbreviations:

AD: Alzheimer's disease; aMCI: amnestic mild cognitive decline; AVLT: the auditory verbal learning test; AVLT-I: AVLT-immediate recall; AVLT-D: AVLT-delayed recall; AVLT-R: AVLT-recognition; ADL: Activities of Daily Living; AAL: automated anatomical labeling; AUC: area under the curve; CSF: cerebrospinal fluid; DWIs:

diffusion weighted images; DMN: default mode network; DTI: diffusion tensor imaging; ECN: executive-control network; FA: fractional anisotropy; HAMD: the Hachinski ischemic scale, the Hamilton depression rating scale; MD: mean diffusivity; MoCA: the Montreal Cognitive Assessment; MPRAGE: magnetization-prepared rapid gradient echo; mPFC: the medial prefrontal cortex; PPC: the posterior cingulate cortex; ReHo: regional homogeneity; ROIs: regions of interest; ROC: receiver operating characteristic; SCD: subjective cognitive decline; SN: salience network; SVM: support vector machine; rs-fMRI: resting-state fMRI;

Introduction:

Alzheimer's disease (AD) is one of the most common progressive and irreversible neurodegenerative diseases. The identification of patients in the early stages of AD has been fundamental for the treatment and possible intervention or prevention before the irreversible cognitive injury. As a result, mild cognitive impairment (MCI) was introduced as the transitional period between normal aging and AD (Dufouil et al., 2005; Glodzik-Sobanska et al., 2007; Jessen et al., 2010; Petersen et al., 1999; van Oijen et al., 2007). In addition, people with amnestic MCI (aMCI) who have progressive symptoms and particular impairments in episodic memory have been reported to be more likely to progress to AD (Cooper et al., 2015). However, the early treatment trials for aMCI patients were disappointing. To stop the disease process, treatment and intervention may need to be initiated even before the onset of MCI. To investigate the pathology of AD during a stage even earlier than MCI, subjective cognitive decline (SCD) was further introduced as a preclinical stage of AD, which is characterized by increasing compensatory cognitive efforts and subtle cognitive decline (Jessen et al., 2014; Reisberg et al., 2010). Extending the early stage of the disease from AD to MCI and then to SCD once again shows the need and importance of early-stage identification of AD (Cheng et al., 2017).

Because of the significance of early-stage identification of AD, SCD and aMCI often serve as important symptomatic indicators of preclinical AD by researchers for early-stage diagnosis and treatment (Davatzikos et al., 2008). Currently, the diagnosis of SCD has largely been based on self-reported symptoms and clinical signs. Investigating the pathological mechanism and accurate biomarker of SCD and the pathological development of AD is clearly an international imperative.

Recently, there has been an explosion of studies investigating AD pathology from a functional or structural perspective. From a functional perspective, by modeling the brain as complex functional networks using functional magnetic resonance imaging (fMRI) data, many studies have achieved significant results. Of these functionally specific networks, the default mode network (DMN), executive-control network (ECN), and salience network (SN) have received the most attention (Bressler and Menon, 2010; Cocchi et al., 2014). Numerous studies have reported that the DMN is highly related to AD (Garces et al., 2014; Greicius et al., 2004). From a structural perspective, by using diffusion tensor imaging (DTI), a quantitative MRI technique that has been applied to detect alterations in white matter, there have also been many studies investigating the

structural connectivity alterations in AD (Amlien and Fjell, 2014; Molinuevo et al., 2014). Several parameters can be derived from DTI data to describe different aspects of diffusion tensors. Fractional anisotropy (FA) and mean diffusivity (MD) characterize the water diffusion in the tissue and are used to describe the white matter structural integrity and to construct the whole-brain anatomical networks (Beaulieu, 2002; Behrens and Sporns, 2012). The characterization of the human brain from a network perspective provides a comprehensive understanding of the structural and functional architectures of the human brain. Mapping and quantifying the connectivity patterns of the human brain (i.e., the human connectome) have become very important topics in the field of neuroscience (Kelly et al., 2012; van den Heuvel et al., 2012), which suggests that cognitive decline in patients with AD is not only caused by damage to a single or local brain region but also by changes in several brain areas and their interactions. In addition to brain connectome changes in the neo-cortical structures, there have also been some studies reporting damage in subcortical structures, including the basal nuclei and the thalamus (de Jong et al., 2008; Jack et al., 2008), suggesting that, in addition to neo-cortical damage, deep gray matter structures in AD suffer severe damage as well.

In the neuroimaging field, machine learning methods, as data-driven techniques, have become powerful tools for classification and pattern analysis studies. With the advantage of their multivariate property, machine learning methods can be applied for whole-brain connectivity analysis and, unlike those analyzing several predefined regions or networks of interest, can ensure the optimal use of the wealth of information present in the brain imaging data. In particular, multivariate pattern analysis methods can both find potential neuroimaging-based biomarkers to differentiate patients from healthy controls at the individual level and potentially detect exciting spatially distributed information to further highlight the neural mechanisms underlying the behavioral symptoms of SCD. In recent years, there has been an increasing amount of interest in multivariate pattern analysis methods to categorize neurodegenerative patients from healthy controls using structural or functional brain images (Chen et al., 2011; Chen et al., 2017; Colliot et al., 2008). In addition, multimodal imaging studies can integrate different modalities of imaging information for analysis. There are several studies that have used machine learning methods combined with multimodal imaging data that have achieved many valuable results (Dyrba et al., 2015a; Fornito and Bullmore, 2010; Teipel et al., 2015; Xu et al., 2015; Zhang et al., 2012). Among these studies, Zhang et al. adopted the regional homogeneity (ReHo) characteristic of fMRI as a classification feature and achieved an accuracy of 71.4% (Zhang et al., 2012). Chen et al. used Fisher linear discriminant analysis, based on the coefficients of a large-scale

network, and yielded an accuracy of 91% (Chen et al., 2011). There are also numerous recent studies that have suggested that effectively integrating information from multimodal imaging data can significantly improve the classification performance (Apostolova et al., 2010; Zhang et al., 2011). Wee et al. and Dyrba et al. applied a multi-kernel support vector machine (SVM) to a multimodal imaging classification study for aMCI and AD participants and obtained clear improvements in accuracy (Dyrba et al., 2015b; Wee et al., 2012).

Considering the promising results from AD pattern analysis and the advantage of machine learning methods, we intend to further apply machine learning methods to the study of the pathological development of AD, which can also provide a potential biomarker for early-stage AD diagnosis. This study can also build a new perspective for combining machine learning methods with the study of brain pathological mechanism.

In this study, we applied machine learning methods to SCD, aMCI and AD pattern analysis. Considering the robust heterogeneity of SCD, we employed a multimodal kernel SVM with multimodal imaging data to improve the accuracy and provide multiple perspectives for our analysis. Specifically, diffusion tensor imaging (DTI) and resting-state fMRI (rs-fMRI) data were applied in our study, which can provide both structural and functional brain connectome information.

Material and Methods:

To extract efficient features from two imaging modalities (DTI and rs-fMRI), we applied brain imaging data to build a connectome matrix. After that, we conducted a feature selection step using the elastic net method. Finally, we implemented multimodal data fusion by using a multimodal SVM algorithm. To explore the pathological mechanism of the entire development from SCD to AD and to verify the generalizability of our method, we applied not only SCD group imaging data but also imaging data from aMCI and AD groups. In this study, we utilized BrainNet Viewer (Xia et al., 2013) and CIRCOS (Krzywinski et al., 2009) for our results visualization.

1. Participants and data acquisition

A total of 167 right-handed, Han Chinese participants were enrolled in this study from September 2009 to December 2015. Among these participants, 45 normal control (NC) participants were recruited from the local community via advertisements and 122 participants with memory concerns were recruited from the memory clinic of the Neurology Department of Xuan Wu Hospital in Beijing, China, including 39 SCD participants, 45 aMCI participants, and 38 AD participants. This study was approved by the Medical Research Ethics Committee and the Institutional Review Board of Xuan Wu Hospital (Clinical Trials.gov identifier: NCT02353884 and NCT02225964). All participants were provided with written informed consent, which they signed prior to any experimental procedures. All participants underwent a series of standardized clinical evaluations, including a medical history interview, neurologic examination, and a string of neuropsychological tests. The neuropsychological tests included the Chinese version of the Mini–Mental State Examination (MMSE), the Beijing version of the Montreal Cognitive Assessment (MoCA) [30], the Clinical Dementia Rating Scale (CDR) [31], the auditory verbal learning test (AVLT) [32], Activities of Daily Living (ADL), the Hachinski ischemic scale, the Hamilton depression rating scale (HAMD) [33], and the Center for Epidemiologic Studies depression scale, among others [34]. The diagnosis was performed by experienced neurologists. All the participants were diagnosed according to specific guidelines and asked to undergo a brain MRI scan once they were enrolled. The demographic details and participant scores on the MMSE are summarized in Table 1.

Table 1 | Group characteristics and participant demographics

	AD	aMCI	SCD	NC	*P* value
No. of participants (female/male)	23/15	23/22	22/17	28/17	0.724[a]
Age (SD) in years	66.22 (8.72)	66.51 (8.83)	66.06 (7.15)	66.02 (6.15)	0.991[b]
Years of education (SD)	8.55 (4.94)	9.78 (5.14)	11.87 (4.24)	10.78 (5.16)	0.023[b,c]
MMSE (SD)	16.92 (6.58)	24.71 (4.00)	28.03 (1.93)	28.00 (2.31)	0.000[b]
MoCA (SD)	13.09 (5.48)	19.66 (4.38)	25.47 (2.55)	26.18 (3.53)	0.000[b]
AVLT-Immediate Recall Scores (SD)	3.52 (1.68)	6.19 (1.72)	8.14 (1.86)	9.25 (1.93)	0.000[b]
AVLT- Delayed Recall Scores (SD)	1.14 (1.75)	3.91 (2.87)	8.74 (2.49)	10.09 (3.07)	0.000[b]
AVLT- Recognition Scores (SD)	3.49	7.82	11.23	11.98	0.000[b]

		(3.16)	(4.01)	(2.69)	(2.66)

Note: $p<0.05$ means significance existed between groups.

a The *P* value for sex distribution was obtained by chi-square test.

b The *P* values were obtained by ANOVA analysis.

c Significance only exists between SCD group and AD group. No significance exists between normal controls and other groups.

The NC participants were required to meet the following research criteria: (a) no memory concerns; (b) MMSE and MoCA scores within the normal range (adjusted for age, sex, and education); and (c) a CDR score of 0.

The diagnosis of SCD met the following published SCD research criteria proposed by the Subjective Cognitive Decline Initiative (SCD-I): (a) self-perceived continuous decline in memory compared with the previous normal status within the last 5 years combined with informant report; (b) MMSE and MoCA scores within the normal range after age, gender, and education adjustments; and (c) a CDR score of 0.

The inclusion criteria for aMCI included the following: (a) memory complaint, confirmed by an informant; (b) objectively impaired memory confirmed by neuropsychological tests; (c) clear-cut history of cognitive worsening; (d) failure to meet the criteria for dementia according to the Diagnostic and Statistical Manual of Mental Disorders, Fourth Edition, revised (DSM-IV-R); and (e) a CDR score of 0.5.

The AD participants were diagnosed according to the National Institute of Aging-Alzheimer's (NIA-AA) criteria for clinically probable AD: (a) a condition meeting criteria for dementia; (b) insidious and gradual onset (not sudden) over more than 6 months; (c) clear-cut history of worsening cognition; (d) the initial and most prominent cognitive deficits evident in the performance of amnestic presentation or nonamnestic presentations; and (e) hippocampal atrophy confirmed by structural MRI.

The exclusion criteria applied to all participants and included the following: (a) a history of stroke (Hachinski ischemic scale score > 4 points); (b) severe depression (HAMD score > 24 points or the Center for Epidemiological Studies Depression Scale score > 21 points); (c) other central nervous system diseases that could cause cognitive decline (e.g., epilepsy, brain tumors, Parkinson's disease, or encephalitis); (d) systemic diseases, which could cause cognitive impairment (e.g., anthracemia, syphilis, thyroid dysfunction, severe anemia, or HIV); (e) a history of psychosis or congenital mental growth retardation; (f) severe hypoplasia or dysacusis; (g) cognitive decline caused by

traumatic brain injury; (h) severe end-stage diseases or severe diseases in the acute stages; or (i) inability complete the neuropsychological tests or contraindications to MRI.

All MR scans were performed on a 3.0 Tesla MR system (Siemens Magnetom Trio Tim MRI system, Germany) using a standard head coil. During the entire scanning procedure, cushions and headphones were used to reduce participant motion and scanner noise, respectively. Structural DTI data, T1-weighted data and functional rs-fMRI data were available for all participants.

The DTI data were collected using an echo planar imaging (EPI) sequence three times with the following parameters: 31 independent, noncollinear directions of a b-value = 1000 s/mm^2 and one additional image with no diffusion weighting (b = 0), slices = 60, repetition time (TR) = 11000 ms, echo time (TE0 = 98 ms, flip angle = 90°, field of view (FOV) = 256 mm × 232 mm, acquisition matrix = 128×116, and thickness = 2 mm with reversed k-space readout. The resulting T1-weighted images and cortical models were linearly aligned to the space of the diffusion weighted images (DWIs). The DWIs, as well as the resulting tracts, were further elastically registered to the T1-weighted images to account for susceptibility artifacts.

Resting-state blood oxygenation level-dependent (BOLD) signals were collected using a gradient EPI sequence: 28 axial slices; TR = 2000 ms; TE = 40 ms; flip angle = 90°; slice thickness = 4.0 mm; gap = 0.8 mm; matrix = 64 × 64; and FOV = 256 × 256 mm2. During scanning, the participants were instructed to keep their eyes closed, relax their minds, and remain motionless as much as possible but to not fall asleep. The rs-fMRI scan lasted for 8 minutes.

Anatomical T1. In addition, a T1-weighted image was acquired for anatomical reference. T1-weighted MR images were obtained by a 3D magnetization-prepared rapid gradient echo (MPRAGE) sequence with the following parameters: slices = 176, TR = 1900 ms, TE = 2.2 ms, inversion time (TI) = 900 ms, flip angle = 9°, FOV = 256 mm^2, acquisition matrix = 224 × 256, no gap, and thickness = 1.0 mm.

2. Network construction

The preprocessing of the DTI data and structural brain connectome matrix construction steps were performed via PANDA (Cui et al., 2013), which is a pipeline toolbox for

analyzing brain diffusion imaging. The FA of each voxel was computed. Affine transformation was used to coregister the FA images in native space to their corresponding T1-weighted images. The structural images were then nonlinearly registered to the ICBM152 template. Based on the above two steps, an inverse warping transformation from the standard space to the native MRI space can be obtained. The automated anatomical labeling (AAL) atlas in the standard space was then inversely warped back to the individual native space by applying this inverse transformation. This parcellation divided the cortical surface into 90 regions (45 per hemisphere). The resulting inverse deformation map ($\square^{-1}$) for each participant was then applied to warp the AAL template to the DTI native space of each participant, using the nearest neighbor interpolation method, as each AAL region was defined as a structural brain network node.

Finally, for each individual, white matter pathways were reconstructed and referred to as fibers or tracts using streamline tractography. The fiber assignment by continuous tracking (FACT) algorithm was used. In the brain mask, 8 seeds followed the main diffusion directions from voxel to voxel; a streamline was terminated when it reached a voxel with an FA value lower than 0.1 (reflecting low levels of preferred diffusion, often gray matter voxels), when the streamline exceeded the brain mask (i.e., gray and white matter voxels), or when the trajectory of the streamline made a turn sharper than 45 degrees. Streamlines longer than 15 mm were considered for further analysis. In the end, we obtained the brain connectome matrix for each individual.

The preprocessing of the rs-fMRI data and functional brain connectome matrix construction steps were performed via GRETNA (Wang et al., 2015), which is an efficient graph theoretical network analysis toolbox for imaging connectomics.

Preprocessing of the rs-fMRI, such as slice timing correction and head-motion correction were performed using the Statistical Parametric Mapping software package (SPM8, http://www.fil.ion.ucl.ac.uk.spm). To ensure magnetization equilibrium, the first 10 acquired fMRI images of each participant were discarded. The remaining 140 images were first corrected for the acquisition time delay among different the slices before they were realigned to the first volume of the remaining images for head-motion correction. We hypothesized that the variability in the BOLD signal of the gray matter regions is sensitive for delineating alterations in the connectivity patterns caused by pathological attacks of SCD. Removing the signal from the ventricles and white matter is motivated by the fact that these regions contain a relatively high proportion of noise caused by the cardiac and respiratory cycles. Accordingly, we first segmented the T1-

weighted image of each participant into gray matter, white matter and cerebrospinal fluid (CSF). For each participant, the gray matter was then used to mask the fMRI images. This procedure eliminated the possible contribution of the white matter and CSF to the rs-fMRI time series.

The first scan of the fMRI time series was coregistered to the T1-weighted image of the same participant. The estimated transformation was then applied to other fMRI scans of the same participant. Deformation fields were estimated by warping the AAL template (Tzourio-Mazoyer et al., 2002) (T1-weighted imaging) to the participant's T1-weighted images using a deformable registration method called HAMMER (Wu et al., 2014). The brain space of each participant was then parcellated into 90 regions of interest (ROIs) by warping the AAL region masks to the participant space using the estimated deformation fields. For each participant, the mean time series of each individual ROI was computed by averaging the gray matter-masked fMRI time series over all voxels in that particular ROI.

One crucial step in rs-fMRI analysis is temporal bandpass filtering. The frequency interval of bandpass filtering varies and depends on the application but is normally within the interval of 0.01-0.10 Hz since the fMRI dynamics of neuronal activities are most salient within this frequency interval. Temporal bandpass filtering provides a reasonable trade-off between avoiding the physiological noise associated with higher-frequency oscillations and the measurement error associated with estimating very low-frequency correlations from limited time series.

Functional connectivity, which represents interregional correlations in neuronal variability, was measured using pairwise Pearson correlation coefficients between the ROI pairs. Given a set of N random variables, the Pearson correlation matrix is a symmetric matrix in which each off-diagonal element is the correlation coefficient between a pair of variables. We considered the brain regions as a set of nodes and the correlation coefficients as signed weights represented by the edges connecting the nodes. Fisher's r-to-z transformation was applied on the elements of the Pearson correlation matrix to improve the normality of the correlation coefficients. The functional connectivity networks were represented in the form of z-maps. Hence, the structural and functional brain connectome matrix for each individual was ultimately obtained, which are 90×90 symmetric matrixes.

3. Data preprocessing

The main procedures after brain connectome construction are shown in Fig. 1. After network construction, we performed data cleaning and normalization steps. Given the individual variability in brain anatomy (Amunts et al., 1999), anatomical connectivity between regions often differs across participants. In this study, we focused on the connections that were most consistent across participants, that is, the backbone network. To identify the highly consistent cortical connections, we applied a nonparametric one-tailed sign test (Gong et al., 2009). For each pair of cortical regions, the sign test was performed with the null hypothesis that there was no existing connection, that is, 'fiber bundle number = 0'. The Bonferroni method was used to correct for multiple comparisons (i.e., 89 × 90/2 = 4005 pairs of regions) at $P < 0.05$. The sign test was chosen because of doubts about the validity of the absolute fiber bundle number estimates and to minimize inclusion of false positives. The use of this conservative statistical criterion generated a symmetric weighted matrix that captured the underlying anatomical connectivity patterns in the human cerebral cortex. After the sign test, there were 1649 DTI matrix values and 1058 fMRI matrix values left. These matrix values were then converted into row vectors for the next feature selection stage.

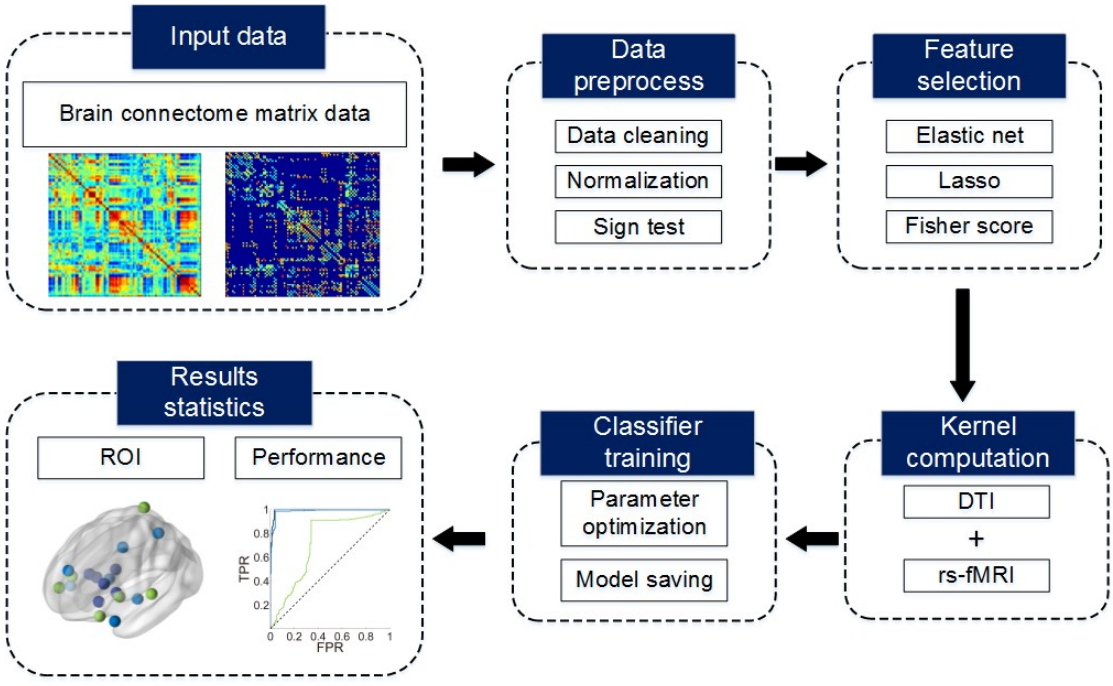

Figure 1 | Main procedure after brain connectome construction. The procedure included six parts: (1) input data; (2) data preprocess; (3) feature selection; (4) kernel computation; (5) classifier training; and (6) results statistics.

3. Feature selection

The feature-selection procedure was developed to select a subset of the original features. We employed the elastic net method for our feature selection. Notably, we also employed two other feature-selection methods, the Fisher score and lasso methods, for comparison.

A promising technique called the lasso was proposed by Tibshirani (1996). The lasso is a penalized least squares method that imposes an L1 penalty on the regression coefficients. Due to the nature of the L1 penalty, the lasso performs both continuous shrinkage and automatic variable selection simultaneously. Moreover, Hui Zou's team proposed a new regularization technique called the elastic network, which is similar to the lasso but with fewer limitations and, thus, is more widely used. In our study, we applied this method for our feature-selection procedure (Zou and Hastie, 2005). We employed two circulations in our code to determine the optimal norm regularization parameters L1 and L2.

The Fisher score is a univariate filter method commonly employed to determine the discriminatory power of individual features between two classes of equal probability (Yilmaz, 2013)[44][1]. Moreover, it is independent of the class distribution. Therefore, if the data are not normally distributed, users can choose this option instead (Khazaee et al., 2016)[45][2]. We employed one circulation in our code to determine the optimal threshold parameters, *p*.

4. Multimodal SVM algorithm

SVM, as parametrically kernel-based method for addressing supervised classification problems, have been proven to be successful in many fields (Su et al., 2007). Recent developments have shown the benefits of a multimodal SVM (Nan et al., 2009; Wee et al., 2012). A multimodal SVM adequately utilizes the particular characteristics of each modality's data and provides more possibilities to choose a suitable weighted combination, especially for data from multiple heterogeneous sources. The kernel function is defined as follows:

$$K(x_i, x_j) = \left\langle \Phi(x_i), \Phi(x_j) \right\rangle \quad (1)$$

The kernel function is K; $\boldsymbol{x}_i$, $\boldsymbol{x}_j$ are the input vectors; and Φ is a map to transform the source data from the input space to feature space. Kernel function has many different forms, including Gaussian, linear, polynomial, etc. In (1), the scalar value K can describe the distance or similarity of the two feature vectors in high dimensions, which shows the advantages in the linear inseparable problem. In our study, we choose linear kernel which is commonly used for high dimension feature (Inano et al., 2014). The final kernel function combined with the multimodal data source with a weight coefficient has a form of

$$K(x_i, x_j) = \beta_1 K_1(x_{i1}, x_{j1}) + \beta_2 K_2(x_{i2}, x_{j2}) \quad (2)$$

$\{\boldsymbol{\beta}_n\}$ is the weight coefficient. $\boldsymbol{K}_n$ is the kernel function of each modality's data $\boldsymbol{x}^n$. M data samples and two modality kernels are used in the learning. The decision function in the classification with a best parameter set is defined as follows:

$$\hat{y}(x) = \sum_{m=1}^{M} \alpha_m y_m K(x, x_m) + b \quad (3)$$

$\{\boldsymbol{\alpha}_m\}$ is a weight series. $\boldsymbol{y}_m$ is the label of the sample. $\boldsymbol{x}_m$.K is the final kernel defined before, and $\boldsymbol{b}$ is a constant coefficient. It can be noticed that the $\boldsymbol{K}$ is different from that in equation (2) because it was used for prediction.

In our study, we utilized a multimodal SVM algorithm based on a linear kernel to integrate the multimodal brain connectome information. The DTI network and rs-fMRI network represent the structural and functional information of the brain connectome. The β_n was introduced to denote the weight of the two modalities. Due to our limited number of samples, a k-fold cross-validation approach was implemented. Specifically, the dataset was randomly partitioned into 10 non-overlapping subsets; 9 out of the 10 subsets were used for training, whereas the remaining one was used for testing. To further avoid possible biases during partitioning, we repeated the experiments 10 times. In each experiment, we employed inner iterations to determine the feature selection parameters, the model parameters and the modality weights β in the multi-kernel SVM. After all the model-training experiments, we counted the frequency of each selected feature in all experiments and the frequencies of the brain regions according to their related connectivity features. The SVM algorithm in our study was based on the

LIBSVM library toolbox (http://www.csie.ntu.edu.tw/~cjlin/libsvm) (Chang and Lin, 2011) within the MATLAB environment.

Results:

1. Classifier performance comparison

To verify the advantage of the multimodal pattern analysis method, the comparison experiments of multimodal and single-modal methods were taken. The performance was summarized in Table 2. We can also see the performance differences among the three feature-selection methods. In the SCD group experiment, we obtained a cross-validated accuracy of 77.02% for the Fisher score, 76.78% for the lasso, and 80.24% for the elastic net. In the aMCI group, we obtained a cross-validated accuracy of 95.93% for the Fisher score, 96.69% for the lasso, and 97.76% for the elastic net. In the AD group, we obtained a cross-validated accuracy of 98.26% for the Fisher score, 98.77% for the lasso, and 98.58% for the elastic net.

Table 2 | Classification performance of multimodal and single-modal methods (Multi: DTI + fMRI; Accuracy: %)

Group		SCD			aMCI			AD	
modality	DTI	fMRI	Multi	DTI	fMRI	Multi	DTI	fMRI	Multi
Elastic net	58.51	77.81	80.24	95.78	84.33	97.76	93.60	95.71	98.58
Lasso	56.98	72.09	76.78	94.58	81.09	96.69	93.10	94.62	98.77
Fisher score	63.36	72.89	77.02	94.27	83.38	95.93	93.20	92.61	98.26

Moreover, the two kinds of receiver operating characteristic (ROC) curves are shown in Fig. 2: the comparison of different feature-selection methods in the SCD group experiment and the different group experiments using the elastic net method.

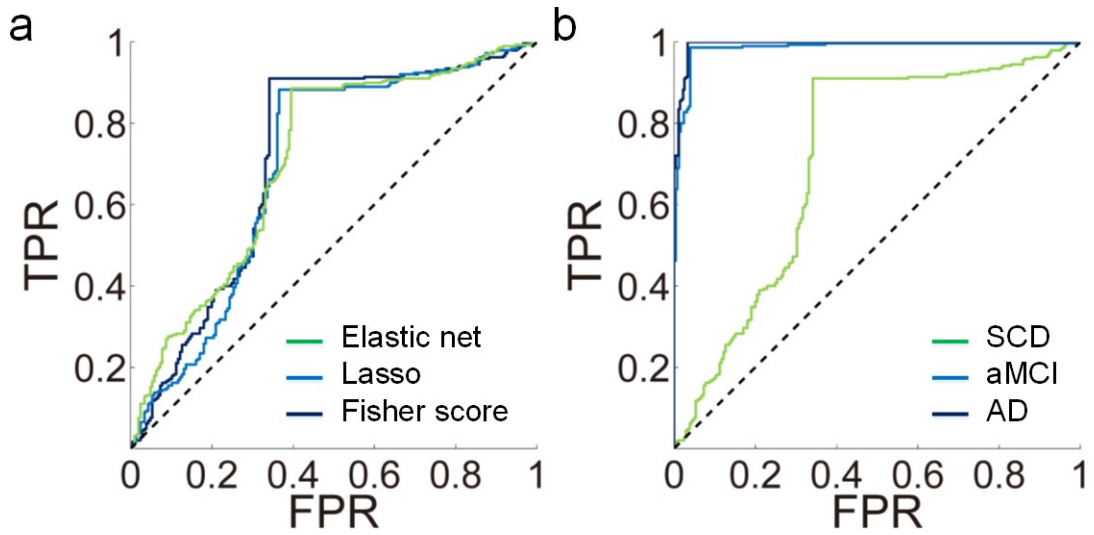

Figure 2 | ROC curve comparison. (a) The SCD classification experiment with different feature-selection methods. The area under the curve (AUC) values in this experiment were as follows: elastic net, 0.7154; lasso, 0.6939; and Fisher score, 0.7098. (b) Different group classification experiments using the elastic net. The AUC values in this experiment were as follows: SCD, 0.7154; aMCI, 0.984; and AD, 0.9940.

Connectivity statistics analysis

In the end, we summarized the most significative brain regions in the SCD, aMCI and AD classification experiments using our proposed method. In each experiment, we employed 10-fold cross-validation approach and repeated it 10 times. For each fold validation iteration result, we can get the best feature subset corresponding to optimal SVM classifiers we've trained. Each feature represents the connectivity between two brain regions. So after the 100 iterations, we computed the frequency of each feature being selected and the brain regions' frequencies according to their related connectivity feature and arranged the brain regions' frequencies from high to low.

After that, we attempted to use a reasonable threshold to select the high-frequency brain regions, which were indicated to have high discriminative power. However, there are few related studies that we could refer to. Therefore, we conducted a normality test of the statistical results and found that the frequency results followed a normal distribution. Therefore, we ultimately took the top twenty brain regions by ourselves according to our needs, which is very common for normal distribution data analysis. The top twenty regions are listed in Table 3. The results in the three group experiments were highly

similar and are as follows: putamen, hippocampus, pallidum, precuneus and many other regions. We discuss the details in the discussion section.

Table 3 | The top twenty significant brain regions

SCD		aMCI		AD	
Name	No.	Name	No.	Name	No.
Frontal.Sup.Orb.L	5	Frontal.Inf.Orb.L	15	Frontal.Inf.Orb.L	15
Frontal.Sup.Orb.R	6	Frontal.Inf.Orb.R	16	Frontal.Inf.Orb.R	16
Frontal.Inf.Tri.R	14	Olfactory.L	21	Olfactory.L	21
Frontal.Inf.Orb.L	15	Olfactory.R	22	Frontal.Sup.Medial.L	23
Frontal.Inf.Orb.R	16	Frontal.Sup.Medial.L	23	Insula.L	29
Supp.Motor.Area.L	19	Insula.L	29	Cingulum.Ant.R	32
Olfactory.L	21	Insula.R	30	Cingulum.Mid.L	33
Frontal.Sup.Medial.R	24	Cingulum.Ant.R	32	Hippocampus.L	37
Frontal.Mid.Orb.R	26	Cingulum.Mid.R	34	Hippocampus.R	38
Cingulum.Mid.L	33	Hippocampus.R	38	Parietal.Sup.R	60
Hippocampus.R	38	Parietal.Sup.R	60	Precuneus.L	67
Amygdala.L	41	Precuneus.R	68	Caudate.L	71
Parietal.Sup.L	59	Putamen.L	73	Caudate.R	72
Precuneus.L	67	Putamen.R	74	Putamen.L	73
Putamen.L	73	Pallidum.R	76	Putamen.R	74
Putamen.R	74	Thalamus.L	77	Pallidum.R	76
Pallidum.R	76	Temporal.Sup.L	81	Thalamus.R	78
Temporal.Sup.L	81	Temporal.Sup.R	82	Temporal.Sup.L	81
Temporal.Sup.R	82	Temporal.Pole.Sup.L	83	Temporal.Pole.Sup.L	83
Temporal.Pole.Sup.L	83	Temporal.Pole.Sup.R	84	Temporal.Pole.Sup.R	84

Table 3 No: the region's serial number in the AAL atlas; L: left; R: right; Sup: superior; Orb: orbital; Inf: inferior; Supp: supplementary; Mid: medial; Ant: anterior

We found that most of these top regions are within the DMN or are SCS. The rest are mainly related to higher-level functions. To show the brain connectome changes with the development of disease, the high-frequency connections in the DMN and SCS are shown in Fig. 3A and Fig. 3B, which was defined as the connectivity appearing in the final feature set more than 90 times in 100 cross-validation iterations. Color balls represent the DMN brain regions, and gray balls represent the other seventy brain regions.

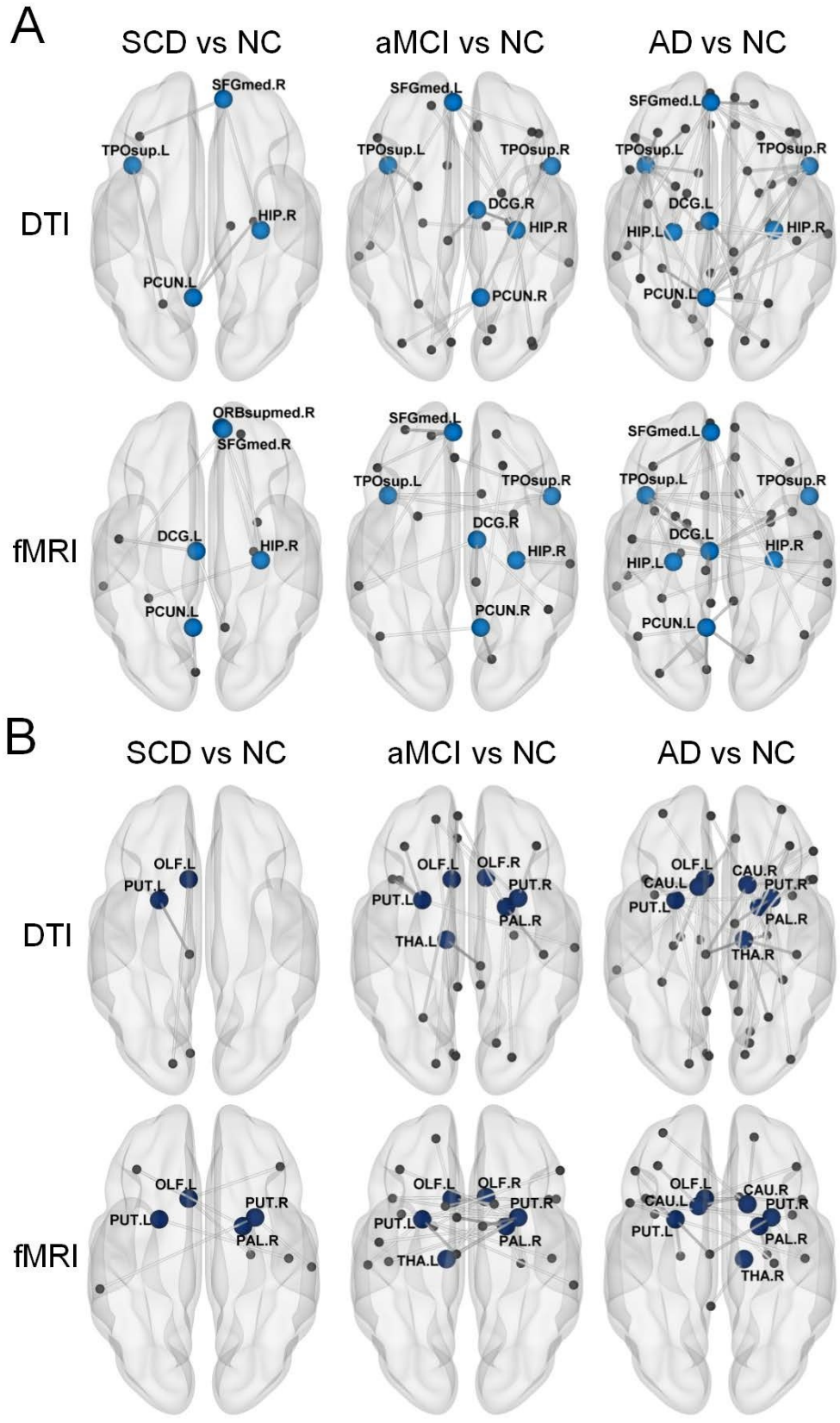

Figure 3 | High-frequency connectivity. (A) The high-frequency connectivity in the DMN. (B) The high-frequency connectivity of the SCS.

The distribution of the brain regions is shown in Fig. 4. In Fig. 5, we illustrate all the high-frequency connectivities related to top brain regions in the three group experiments to show the complete development of AD pathology.

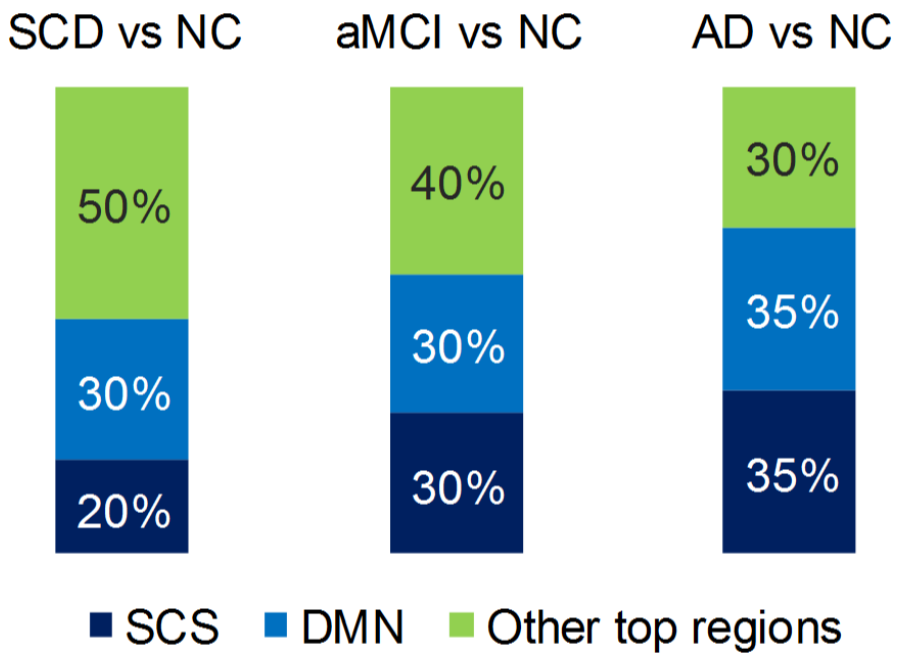

Figure 4 | Distribution of the top twenty regions. The histogram of three kinds of brain regions, and the change trends of the SCS and other top regions are very obvious.

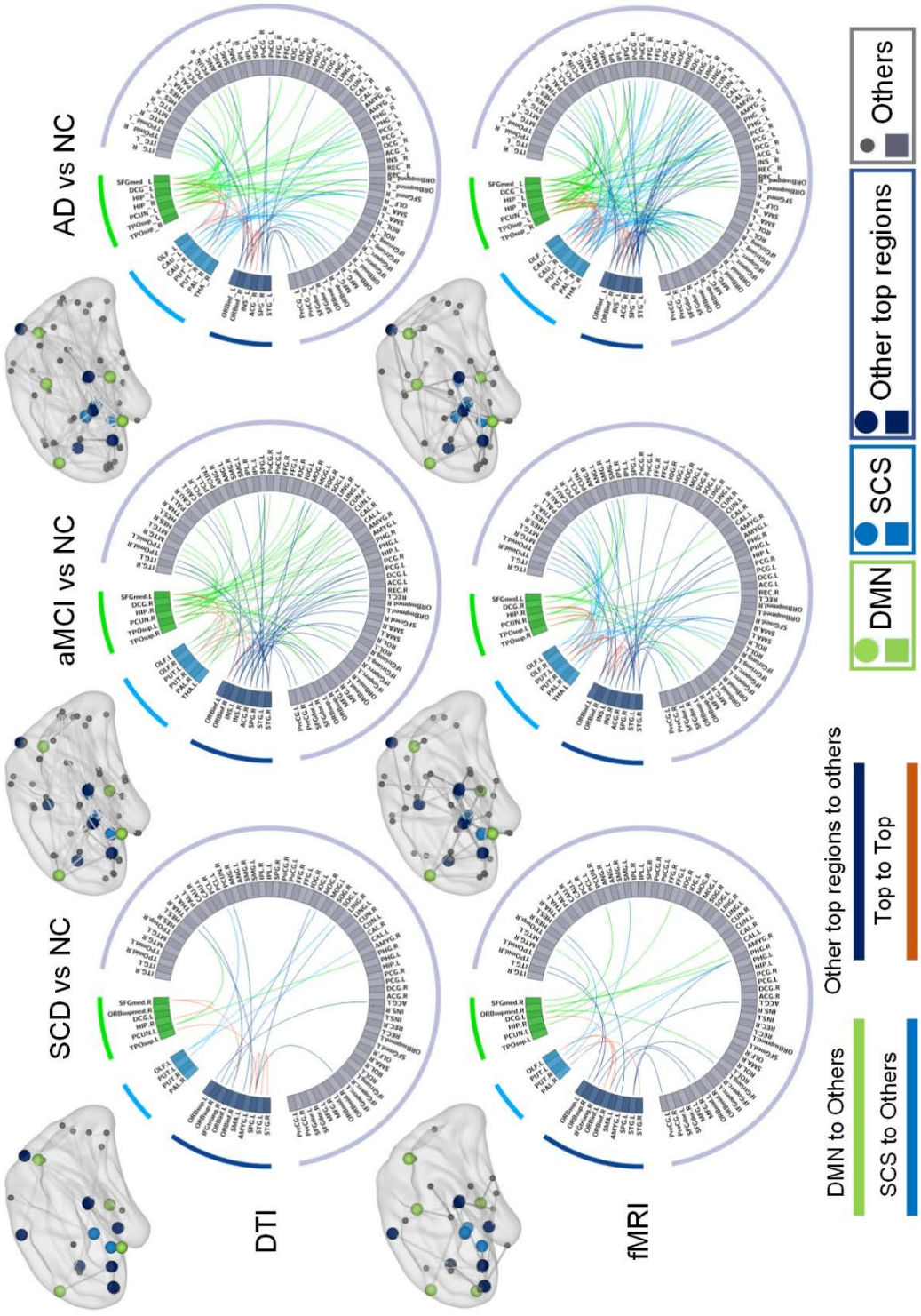

Figure 5 | High frequency connections in three group experiments. In the 3D brain diagram, big color balls represent the three kinds of top regions and small grey balls represent the other seventy brain regions. In the circle diagram, red connections represent the connections among the top twenty regions. The other color connections represent the connections between the three kinds of top regions and the other seventy brain regions.

Discussion:

To investigate AD pathological development and the biomarkers for early-stage AD identification, we applied machine learning methods with neuroimaging data and the brain connectome theory, and we achieved many meaningful results. The majority of the connections and brain regions with high discriminative power were located in the DMN and SCS. In particular, the results of the three group experiments included many of the same brain regions.

As mentioned above, the results of all three groups exhibited significant differences in the DMN. Abnormalities in the DMN can be observed across a range of neurological disorders (Buckner et al., 2008). Many important regions of the DMN were selected, such as the medial part of the superior frontal gyrus, the middle cingulate, the hippocampus, the precuneus, and the superior temporal pole. Specifically, in the AAL atlas, the medial part of the superior frontal gyrus is part of the medial prefrontal cortex (mPFC). The middle cingulate is part of the posterior cingulate cortex (PCC). Abnormalities in the DMN in AD have been reported by several previous studies. The mPFC is regarded as a hub region of the DMN (Whitfield-Gabrieli et al., 2011), and alterations in the mPFC may be related to deficits in self-related processing (Andrews-Hanna et al., 2014). The PCC is one of the most metabolically active regions in the brain and a key structure in the DMN. The connection abnormalities in the PCC in AD aligned with the results of recent studies (Greicius et al., 2004). The hippocampus has been subjected to intense scrutiny in AD, which is associated with a gradual decline in some types of memory, including episodic memory and working memory (Hampel et al., 2008). The precuneus is involved in the processing of visual, sensorimotor, and attentional information and has been documented to exhibit decreased DMN connectivity in patients with mild or preclinical AD (Simic et al., 2014). The selected high-frequency connectivity related to the DMN regions is shown in Fig. 3A.

In addition to the DMN regions, another important kind of region that was selected was the SCS, which included the basal nuclei and the thalamus. Specifically, the olfactory cortex, the caudate nucleus, the putamen, the globus pallidus, and the thalamus were found to be significant in our study. In the AAL template, the olfactory cortex consists of part of the striatal area, which is also part of the SCS. The basal nuclei and thalamus are known to participate in many different neuronal pathways, with functions that are not only restricted to motor behavior but are also related to emotional, motivational, associative and cognitive abilities (Herrero et al., 2002). The putamen has been found

to be correlated with AD since amyloid deposits are present early in the disease process (Braak and Braak, 1990; de Jong et al., 2008). Furthermore, the putamen has been correlated with the emergence of dementia in other neurodegenerative disorders, such as Parkinson's disease, due to dopaminergic or other neurochemical deficits (Emre, 2003), indicating once more that its effect on cognitive impairment might be greater than previously assumed. Our study indicated that SCS are very important in the very early stages of AD pathological development. The selected high-frequency connectivity related to the SCS is shown in Fig. 3B.

As a typical neurodegenerative disease, the pathological development of AD was also our study's focus. In Fig. 4, there were some interesting gradients in the SCS and other top regions. With the development of AD pathology, there were more SCS selected as top regions. In contrast, other top regions, which are mainly related to higher-level functions, decreased from 10 to 6. Apart from these regions, the number of DMN regions in among the three group experiments was very stable. We speculated that, in the early stage of AD, the higher-level functional regions are first affected, and with the pathological development of AD, gray matter structures are affected more severely. Specifically, the thalamus, which consists of multiple nuclei and is classically metaphorized as an active relay center, first arose in the aMCI group results. In addition, the thalamus serves both sensory and motor functions (de Jong et al., 2008; Herrero et al., 2002). The caudate nucleus first arose at AD group results. The caudate nucleus has long been associated with various other cognitive functions, including memory, procedural learning, associative learning, and inhibitory control of action (Hannan et al., 2010; Seger and Cincotta, 2005). The atrophy in the caudate nucleus in AD and other neurodegenerative diseases has been confirmed by previous studies (Almeida et al., 2003; Barber et al., 2002). Our results indicated that the caudate nucleus may be influenced later than other SCS. Regarding the DMN regions, their results in the three group experiments were very stable, indicating that the DMN regions play an important role throughout the entire development of AD pathology.

In our modality classification experiment, the fMRI and DTI experiments showed significant differences. As shown in Table 2, in the SCD group, the fMRI experimental results were higher than those of the DTI experiment. In the aMCI group, the DTI experimental results became higher even than those of the fMRI experiment. In Fig.3, only SCD group's top brain regions show differences between DTI and fMRI, and there are more top brain regions appearing in fMRI results. We speculated that, in SCD, the very early stage of AD, the brain's functional changes are more significant than the structural changes. In other words, in early-stage AD, the functional damage appeared

earlier than the structural damage, which was consistent with the findings of previous studies (Sun et al., 2016). When it came to the aMCI stage, the structural damage became more severe.

As we can see in Table 3, the results of the SCD group were highly similar to those of the AD and aMCI groups. Notably, there were more superior frontal gyral areas in the SCD group results that are part of the frontal lobe, thus indicating the importance of the frontal lobe in the early diagnosis of AD. In addition, these regions are mainly related to higher-level functions. Moreover, the amygdala was only present in the SCD group results. In the AD and aMCI groups, the ranking of the amygdala fell out of the top twenty regions. The amygdala is very important in many neurodegenerative diseases, and our results indicated that the amygdala had been affected at the very early stage of AD.

In our study, we computed the frequency of each selected feature and arranged the frequencies from high to low. In addition to the brain region statistics, we also selected the high-frequency connections related to the top twenty regions. The results are shown in Fig. 5. In the SCD group, the high-frequency connections were mainly related to the other top regions, which are high-level functionally related. In addition, there were significantly more fMRI high-frequency connections than DTI connections. In addition, with the development of AD pathology, the DTI connections possessed more discriminatory power than those of the fMRI group, which is also consistent with our hypothesis that the functional damage appeared earlier than the structural damage in the SCD stage.

Although our study tried to build a new perspective for the development of AD pathology and early-stage AD identification, a few methodological considerations and directions still require future study. In our study, the accuracy of the SCD group was much lower than those of the AD and aMCI groups because of the high heterogeneity among the SCD patients. Therefore, patient follow-ups can be very essential in SCD studies. If we can obtain more data about SCD patient development, we can achieve more meaningful results regarding the pathophysiological mechanism. On the other hand, we achieved very high accuracy for the AD and aMCI classification study, which implied an overfitting problem due to the very limited number of samples.

In conclusion, we applied multimodal MRI data to investigate the development of AD pathology and a potential biomarker in the early stages of AD. In the three group

experiments, we achieved accuracy values of 80.24% in the SCD group, 97.76% in the aMCI group and 98.58% in the AD group. In addition, we counted the top twenty brain regions that showed the most discriminative power. In addition, the results showed that these regions were mainly located in the DMN and SCS. Moreover, we speculated that, in the early stages of AD, the functional changes appear prior to the structural changes. These insights into the development of AD will provide valuable information regarding early AD diagnosis and pathological mechanism studies.

Acknowledgements:

We gratefully acknowledge all the participants, clinical doctors and researchers at the Department of Neurology, XuanWu Hospital of Capital Medical University.

Funding:

This work was supported by the National Key Research and Development Program of China under grant 2017YFB1002504, the National Natural Science Foundation of China (Grant No. 81671776, 61633018, 61727807), the Beijing Municipal Science & Technology Commission (Z161100002616020, Z131100006813022, PXM2017_026283_000002), the Beijing Nova Program (Grant No. Z171100001117057), the Fundamental and Clinical Cooperative Research Program of Capital Medical University (16JL-L08), the Health and Family Planning Commission of the Shunyi District Beijing, and the Opening Foundation of the Key Laboratory of Behavioral Science, Chinese Academy of Sciences.

References

Almeida, O.P., et al., 2003. MRI study of caudate nucleus volume in Parkinson's disease with and without dementia with Lewy bodies and Alzheimer's disease. Dement Geriatr Cogn Disord. 16, 57-63.

Amlien, I.K., Fjell, A.M., 2014. Diffusion Tensor Imaging of White Matter Degeneration in Alzheimer's Disease and Mild Cognitive Impairment. Neuroscience. 276, 206-215.

Amunts, K., et al., 1999. Broca's region revisited: Cytoarchitecture and intersubject variability. Journal of Comparative Neurology. 412, 319-341.

Andrews-Hanna, J.R., Smallwood, J., Spreng, R.N., 2014. The default network and self-generated thought: component processes, dynamic control, and clinical relevance. Year in Cognitive Neuroscience. 1316, 29-52.

Apostolova, L.G., et al., 2010. 3D PIB and CSF biomarker associations with hippocampal atrophy in ADNI subjects. Neurobiology of Aging. 31, 1284-1303.

Barber, R., et al., 2002. Volumetric MRI study of the caudate nucleus in patients with dementia with Lewy bodies, Alzheimer's disease, and vascular dementia. Journal of Neurology Neurosurgery and Psychiatry. 72, 406-407.

Beaulieu, C., 2002. The basis of anisotropic water diffusion in the nervous system - a technical review. Nmr in Biomedicine. 15, 435-455.

Behrens, T.E., Sporns, O., 2012. Human connectomics. Curr Opin Neurobiol. 22, 144-53.

Braak, H., Braak, E., 1990. Alzheimers-Disease - Striatal Amyloid Deposits and Neurofibrillary Changes. Journal of Neuropathology and Experimental Neurology. 49, 215-224.

Bressler, S.L., Menon, V., 2010. Large-scale brain networks in cognition: emerging methods and principles. Trends in Cognitive Sciences. 14, 277-290.

Buckner, R.L., Andrews-Hanna, J.R., Schacter, D.L., 2008. The brain's default network - Anatomy, function, and relevance to disease. Year in Cognitive Neuroscience 2008. 1124, 1-38.

Chang, C.C., Lin, C.J., 2011. LIBSVM: A Library for Support Vector Machines. Acm Transactions on Intelligent Systems and Technology. 2.

Chen, G., et al., 2011. Classification of Alzheimer disease, mild cognitive impairment, and normal cognitive status with large-scale network analysis based on resting-state functional MR imaging. Radiology. 259, 213-21.

Chen, X., et al., 2017. Extraction of dynamic functional connectivity from brain grey matter and white matter for MCI classification. Hum Brain Mapp. 38, 5019-5034.

Cheng, Y.W., Chen, T.F., Chiu, M.J., 2017. From mild cognitive impairment to subjective cognitive decline: conceptual and methodological evolution. Neuropsychiatric Disease and Treatment. 13, 491-498.

Cocchi, L., et al., 2014. Complexity in Relational Processing Predicts Changes in Functional Brain Network Dynamics. Cerebral Cortex. 24, 2283-2308.

Colliot, O., et al., 2008. Discrimination between Alzheimer disease, mild cognitive impairment, and normal aging by using automated segmentation of the hippocampus. Radiology. 248, 194.

Cooper, C., et al., 2015. Modifiable Predictors of Dementia in Mild Cognitive Impairment: A Systematic Review and Meta-Analysis. American Journal of Psychiatry. 172, 323- 334.

Cui, Z.X., et al., 2013. PANDA: a pipeline toolbox for analyzing brain diffusion images. Frontiers in Human Neuroscience. 7.

Davatzikos, C., et al., 2008. Detection of prodromal Alzheimer's disease via pattern classification of magnetic resonance imaging. Neurobiol Aging. 29, 514-23.

de Jong, L.W., et al., 2008. Strongly reduced volumes of putamen and thalamus in Alzheimers disease: an MRI study. Brain. 131, 3277-3285.

Dufouil, C., Fuhrer, R., Alperovitch, A., 2005. Subjective cognitive complaints and cognitive decline: consequence or predictor? The epidemiology of vascular aging study. J Am Geriatr Soc. 53, 616-21.

Dyrba, M., et al., 2015a. Predicting Prodromal Alzheimer's Disease in Subjects with Mild Cognitive Impairment Using Machine Learning Classification of Multimodal Multicenter Diffusion-Tensor and Magnetic Resonance Imaging Data. Journal of Neuroimaging. 25, 738.

Dyrba, M., et al., 2015b. Multimodal analysis of functional and structural disconnection in Alzheimer's disease using multiple kernel SVM. Human Brain Mapping. 36, 2118- 2131.

Emre, M., 2003. What causes mental dysfunction in Parkinson's disease? Movement Disorders. 18, S63-S71.

Fornito, A., Bullmore, E.T., 2010. What can spontaneous fluctuations of the blood oxygenation-level-dependent signal tell us about psychiatric disorders? Current Opinion in Psychiatry. 23, 239.

Garces, P., et al., 2014. The Default Mode Network is functionally and structurally disrupted in amnestic mild cognitive impairment - A bimodal MEG-DTI study. Neuroimage- Clinical. 6, 214-221.

Glodzik-Sobanska, L., et al., 2007. Subjective memory complaints: presence, severity and future outcome in normal older subjects. Dement Geriatr Cogn Disord. 24, 177-84.

Gong, G.L., et al., 2009. Mapping Anatomical Connectivity Patterns of Human Cerebral Cortex Using In Vivo Diffusion Tensor Imaging Tractography. Cerebral Cortex. 19, 524-536.

Greicius, M.D., et al., 2004. Default-mode network activity distinguishes Alzheimer's disease from healthy aging: Evidence from functional MRI. Proceedings of the National Academy of Sciences of the United States of America. 101, 4637-4642.

Hampel, H., et al., 2008. Core candidate neurochemical and imaging biomarkers of Alzheimer's disease. Alzheimers & Dementia. 4, 38-48.

Hannan, K.L., et al., 2010. Caudate nucleus volume in individuals at ultra-high risk of psychosis: A cross-sectional magnetic resonance imaging study. Psychiatry Research- Neuroimaging. 182, 223-230.

Herrero, M.T., Barcia, C., Navarro, J.M., 2002. Functional anatomy of thalamus and basal ganglia. Childs Nervous System. 18, 386-404.

Inano, R., et al., 2014. Voxel-based clustered imaging by multiparameter diffusion tensor images for glioma grading. Neuroimage Clin. 5, 396-407.

Jack, C., et al., 2008. C-11 PiB and structural MRI provide complementary information in imaging of AD and amnestic MCI. Neurology. 70, A418-A418.

Jessen, F., et al., 2010. Prediction of dementia by subjective memory impairment: effects of severity and temporal association with cognitive impairment. Arch Gen Psychiatry. 67, 414-22.

Jessen, F., et al., 2014. A conceptual framework for research on subjective cognitive decline in preclinical Alzheimer's disease. Alzheimers Dement. 10, 844-52.

Kelly, C., et al., 2012. Characterizing variation in the functional connectome: promise and pitfalls. Trends in Cognitive Sciences. 16, 181-188.

Khazaee, A., Ebrahimzadeh, A., Babajani-Feremi, A., 2016. Application of advanced machine learning methods on resting-state fMRI network for identification of mild cognitive impairment and Alzheimer's disease. Brain Imaging and Behavior. 10, 799-817.

Krzywinski, M., et al., 2009. Circos: An information aesthetic for comparative genomics. Genome Research. 19, 1639-1645.

Molinuevo, J.L., et al., 2014. White matter changes in preclinical Alzheimer's disease: a magnetic resonance imaging- diffusion tensor imaging study on cognitively normal older people with positive amyloid beta protein 42 levels. Neurobiology of Aging. 35, 2671-2680.

Nan, Z., et al., 2009. Multi-kernel SVM based classification for brain tumor segmentation of MRI multi-sequence. In: 2009 16th IEEE International Conference on Image Processing (ICIP 2009), 7-12 Nov. 2009. Proceedings of the 2009 16th IEEE International Conference on Image Processing (ICIP 2009), Vol., ed.^eds. IEEE, Piscataway, NJ, USA, pp. 3373-6.

Petersen, R.C., et al., 1999. Mild cognitive impairment: clinical characterization and outcome. Arch Neurol. 56, 303-8.

Reisberg, B., et al., 2010. Outcome over seven years of healthy adults with and without

subjective cognitive impairment. Alzheimers & Dementia. 6, 11-24.

Seger, C.A., Cincotta, C.M., 2005. The roles of the caudate nucleus in human classification learning. Journal of Neuroscience. 25, 2941-2951.

Simic, G., et al., 2014. Early Failure of the Default-Mode Network and the Pathogenesis of Alzheimer's Disease. Cns Neuroscience & Therapeutics. 20, 692-698.

Su, R., et al., 2007. Tumor segmentation from a multispectral MRI images by using support vector machine classification. In: 2007 4th IEEE International Symposium on Biomedical Imaging: Macro to Nano, 12-15 April 2007. 2007 4th IEEE International Symposium on Biomedical Imaging: Macro to Nano (IEEE Cat No. 07EX1544C), Vol., ed.^eds. IEEE, Piscataway, NJ, USA, pp. 1236-9.

Sun, Y., et al., 2016. Subjective Cognitive Decline: Mapping Functional and Structural Brain Changes-A Combined Resting-State Functional and Structural MR Imaging Study. Radiology. 281, 185-192.

Teipel, S.J., et al., 2015. The relative importance of imaging markers for the prediction of Alzheimer's disease dementia in mild cognitive impairment - Beyond classical regression. Neuroimage Clin. 8, 583-93.

Tzourio-Mazoyer, N., et al., 2002. Automated anatomical labeling of activations in SPM using a macroscopic anatomical parcellation of the MNI MRI single-subject brain. Neuroimage. 15, 273-289.

van den Heuvel, M.P., et al., 2012. High-cost, high-capacity backbone for global brain communication. Proceedings of the National Academy of Sciences of the United States of America. 109, 11372-11377.

van Oijen, M., et al., 2007. Subjective memory complaints, education, and risk of Alzheimer's disease. Alzheimers Dement. 3, 92-7.

Wang, J.H., et al., 2015. GRETNA: a graph theoretical network analysis toolbox for imaging connectomics (vol 9, 386, 2015). Frontiers in Human Neuroscience. 9.

Wee, C.Y., et al., 2012. Identification of MCI Individuals Using Structural and Functional Connectivity Networks. Neuroimage. 59, 2045.

Whitfield-Gabrieli, S., et al., 2011. Associations and dissociations between default and self-reference networks in the human brain. Neuroimage. 55, 225-232.

Wu, G.R., et al., 2014. S-HAMMER: Hierarchical attribute-guided, symmetric diffeomorphic registration for MR brain images. Human Brain Mapping. 35, 1044-1060.

Xia, M.R., Wang, J.H., He, Y., 2013. BrainNet Viewer: A Network Visualization Tool for Human Brain Connectomics. Plos One. 8.

Xu, L., et al., 2015. Multi-modality sparse representation-based classification for Alzheimer's disease and mild cognitive impairment. Comput Methods Programs Biomed. 122, 182-90.

Yilmaz, E., 2013. An Expert System Based on Fisher Score and LS- SVM for Cardiac Arrhythmia Diagnosis. Computational and Mathematical Methods in Medicine.

Zhang, D., et al., 2011. Multimodal classification of Alzheimer's disease and mild cognitive impairment. Neuroimage. 55, 856.

Zhang, Z., et al., 2012. Altered spontaneous activity in Alzheimer's disease and mild cognitive impairment revealed by Regional Homogeneity. NeuroImage. 59, 1429.

Zou, H., Hastie, T., 2005. Regularization and variable selection via the elastic net. Journal of the Royal Statistical Society Series B-Statistical Methodology. 67, 301-320.